Research Article

Inter- and Intrasite Correlations of Large-Scale Parameters from Macrocellular Measurements at 1800 MHz

Niklas Jaldén, Per Zetterberg, Björn Ottersten, and Laura Garcia

ACCES Linnaeus Center, KTH Signal Processing Lab, Royal Institute of Technology, 100 44 Stockholm, Sweden

The inter- and intrasite correlation properties of shadow fading and power-weighted angle spread at both the mobile station and the base station are studied utilizing narrowband multisite MIMO measurements in the 1800 MHz band. The influence of the distance between two base stations on the correlation is studied in an urban environment. Measurements have been conducted for two different situations: widely separated as well as closely located base stations. Novel results regarding the correlation of the power-weighted angle spread between base station sites with different separations are presented. Furthermore, the measurements and analysis presented herein confirm the autocorrelation and cross-correlation properties of the shadow fading and the angle spread that have been observed in previous studies.

1. INTRODUCTION

As the demand for higher data rates increases faster than the available spectrum, more efficient spectrum utilization methods are required. Multiple antennas at both the receiver and the transmitter, so-called multiple input multiple output (MIMO) systems, is one technique to achieve high spectral efficiency [1, 2]. Since multiantenna communication systems exploit the spatial characteristics of the propagation environment, accurate channel models incorporating spatial parameters are required to conduct realistic performance evaluations. Since future systems may reuse frequency channels within the same cell to increase system capacity, the characterization of the communication channel, including correlation properties of spatial parameters, becomes more critical. Several measurement campaigns have been conducted to develop accurate propagation models for the design, analysis, and simulation of MIMO wireless systems [3–9]. Most of these studies are based on measurements of a single MIMO link (one mobile and one base station). Thus, these measurements may not capture all necessary aspects required for multiuser MIMO systems. From the measurement data collected, several parameters describing the channel characteristics can be extracted. This work primarily focusses on extracting some key parameters that capture the most essential characteristics of the environment, and that later can be used

to generate realistic synthetic channels with the purpose of link level simulations. To evaluate system performance with several base stations (BS) and mobile stations (MS), it has generally been assumed that all parameters describing the channels are independent from one link (single BS to single MS) to another [3, 10]. However, correlation between the channel parameters of different links may certainly exist, for example, when one BS communicates with two MSs that are located in the same vicinity, or vice versa. In this case, the radio signals propagate over very similar environments and hence, parameters such as shadow fading and/or spread in angle of arrival should be very similar. This has also been experimentally observed in some work where the autocorrelation of the so-called large scale (LS) is studied. These LS parameters, such as shadow fading, delay spread, and angle spread, are shown to have autocorrelation that decreases exponentially with a decorrelation distance of some tenths of meters [11, 12]. High correlation of these parameters is expected if the MS moves within a small physical area. We believe that this may also be the case for multiple BSs that are closely positioned. The assumption that the channel parameters for different links are completely independent may result in over/under estimation of the performance of the multiuser systems. Previous studies [13–15] have investigated the shadow fading correlation between two separate base station sites and found substantial correlation for

closely located base stations. However, the intersite correlation of angle spreads has not been studied previously. Herein, multisite MIMO measurements have been conducted to address this issue. We investigate the existence of correlation between LS parameters on separate links using data collected in two extensive narrow-band measurement campaigns. The intra- and intersite correlations of the shadow fading and the power-weighted angle spread at the base and mobile stations are investigated. The analysis provides unique correlation results for base- and mobile-station angle spreads as well as log-normal (shadow) fading.

The paper is structured as follows: in Section 2 we give a short introduction to the concept of large-scale parameters and in Section 3 some relevant previous research is summarized. The two measurement campaigns are presented in Section 4. In Section 5, we state the assumptions on the channel model while Section 6 describes the estimation procedure. The results are presented in Section 7 and conclusions are drawn in Section 8.

2. INTRODUCTION TO LARGE-SCALE PARAMETERS

The wireless channel is very complex and consists of time varying multipath propagation and scattering. We consider channel modeling that aims at characterizing the radio media for relevant scenarios. One approach is to conduct measurements and "condense" the information of typical channels into a parameterized model that captures the essential statistics of the channel, and later create synthetic data with the same properties for evaluating link and system-level performance, and so on. Large-scale parameters are based on this concept. The term large-scale parameters was used [3] for a collection of quantities that can be used to describe the characteristics of a MIMO channel. This collection of parameters are termed large scale because they are assumed to be constant over "large" areas of several wavelengths. Further, these parameters are assumed to depend on the local environment of the transmitter and receiver. Some of the possible LS parameters are listed below:

   (i) shadow fading,
  (ii) angle of arrival (AoA) angle spread,
 (iii) angle of departure (AoD) angle spread,
 (iv) AoA elevation spread,
  (v) AoD elevation spread,
 (vi) cross polarization ratio,
(vii) delay spread.

This paper investigates only the shadow fading and the angle spread parameters. Shadow fading describes the variation in the received power around some local mean, which depends on the distance between the transmitter and receiver; see Section 6.1. The power-weighted angle spread describes the size of the sector or area from which the majority of the power is received. The angle spread parameter will be different for the transmitter (Tx) and receiver (Rx) sides of the link, since it largely depends on the amount of local scat-
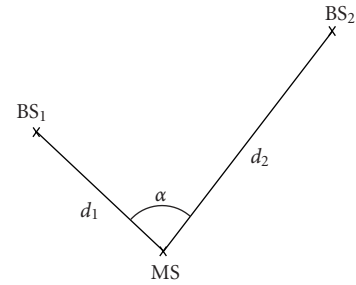

FIGURE 1: Model of the cross-correlation as a function of the relative distance and angle separation, also proposed in [16].

tering; see further in Section 5. A description of the other LS parameters may be found in [3].

3. PREVIOUS WORK

An early paper by Graziano [13] investigates the correlation of shadow fading in an urban macrocellular environment between one MS and two BSs. The correlation is found to be approximately 0.7-0.8 for small angles ($\alpha < 10°$), where α is defined as displayed in Figure 1. Later, Weitzen argued in [14] that the correlation for the shadow fading can be much less than 0.7 even for small angles, in disagreement with the results presented by Graziano. This was illustrated by analyzing measurement data collected in the downtown Boston area using one custom made MS and several pairs of BSs from an existing personal communication system. These results are reasonable since in most current systems the BS sites are widely spread over an area. If the angle α separating the two BSs is small, the relative distance is large, and a small relative distance corresponds to a large angle separation. Thus, a more appropriate model for the correlation of the shadow fading parameter is to assume that it is a function of the relative distance $d = \log_{10}(d_1/d_2)$ between the two BSs and the angle α separating them as proposed in [16]. The distances d_1 and d_2 are defined as in Figure 1. Further studies on the correlation of shadow fading between several sites can be found in, for example, [15, 17–19].

The angular spread parameter has been less studied. In [12], the autocorrelation of the angle spread at a single base station is studied and found to be well modeled by an exponential decay, and the angle spread is further found to be negatively correlated with shadow fading. However, to the authors' knowledge, the intersite correlation of the angle spread at the MS or BS has not been studied previously. Herein, we extend the analysis performed on the 2004 data in [20]. We also investigate data collected in 2005 and find substantial correlation between the shadow fading but less between the angular spreads. The low correlation of the spatial parameters may be important for future propagation modeling. The angle spread at the mobile station is studied and a distribution proposed. Further, we find that the correlation between the base station and mobile station angular spreads (of the same link) is significant for elevated base stations but virtually zero for base stations just above rooftop.

4. MEASUREMENT CAMPAIGNS

Two multiple-site MIMO measurement campaigns have been conducted by KTH in the Stockholm area using custom built multiple antenna transmitters and receivers. These measurements were carried out in the summer of 2004 and the autumn of 2005 and will in the following be refereed to as the 2004 and 2005 campaigns.

Because of measurement equipment shortcomings, the measured MIMO channels have unknown phase rotations. This is due to small unknown frequency offsets. In the 2004 campaign, these phase rotations are introduced at the mobile side and therefore the relation between the measured channel and the true channel is given by

$$\mathbf{H}_{\text{measured, 2004}} = \Lambda_f \mathbf{H}_{\text{true}}, \tag{1}$$

where $\Lambda_f = \text{diag}(\exp(j2\pi f_1 t), \ldots, \exp(j2\pi f_n t))$ and $f_1, \ldots, f_n$ are unknown. Similarly, the campaign of 2005 has unknown phase rotations at the base station side[1] resulting in the following relation:

$$\mathbf{H}_{\text{measured, 2005}} = \mathbf{H}_{\text{true}} \Lambda_f. \tag{2}$$

The frequencies changed up 5 Hz per second. However, the estimators that will be used are designed with these shortcomings in mind.

4.1. Measurement hardware

The hardware used for these measurements is the same as the hardware described in [21, 22]. The transmitter continuously sends a unique tone on each antenna in the 1800 MHz band. The tones are separated 1 kHz from each other. The receiver downconverts the signal to an intermediate frequency of 10 kHz, samples and stores the data on a disk. This data is later postprocessed to extract the channel matrices. The system bandwidth is 9.6 kHz, which allows narrow-band channel measurements with high sensitivity. The offline and narrow-band features simplify the system operation, since neither real-time constrains nor broadband equalization is required. For a thorough explanation of the radio frequency hardware, [23] may be consulted.

4.2. Antennas

In both measurements campaigns, Huber-Suhner dual-polarized planar antennas with slanted linear polarization ($\pm 45°$), SPA 1800/85/8/0/DS, were used at both the transmitter and the receiver. However, only one of the polarizations ($+45°$) was actually used in these measurements. The antennas were mounted in different structures on the mobile and base stations as described below. For more information on the antenna radiation patterns and so on, see [24].
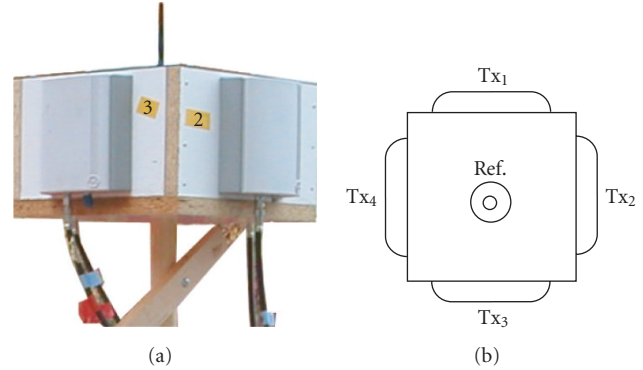

FIGURE 2: Mobile station box antenna.

4.2.1. Base satation array

At the base station, the antenna elements were mounted on a metal plane to form a uniform linear array with 0.56 wavelength (λ) spacing. In the 2004 campaign, an array of four by four elements was used at the BS. However, the "columns" were combined using 4 : 1 combiners to produce four elements with higher vertical gain. The base stations in the 2005 campaign were only equipped with 2 elements.

4.2.2. Mobile station array

At the mobile side, the four antenna elements were mounted on separate sides of a wooden box as illustrated in Figure 2. This structure is similar to the uniform linear array using four elements. A wooden box is used so that the antenna radiation patterns are unaffected by the structure.

4.3. 2004 campaign

In this campaign uplink measurements were made using one 4-element box-antenna transmitter at the MS, see Figure 2, and three 4-element uniform linear arrays (ULA), with an antenna spacing of 0.56λ, at the receiving BSs. The BSs covered 3 sectors on two different sites. Site 1, Kårhuset-A, had one sector while site 2, Vanadis, had two sectors, B and C, separated some 20 meters and with boresights offset 120-degrees in angle. We define a sector by the area seen from the BS boresight $\pm 60°$. The environment where the measurements where conducted can be characterized as typical European urban with mostly six to eight storey stone buildings and occasional higher buildings and church towers. Figure 3 shows the location of the base station sites and the route covered by the MS. The BS sectors are displayed by the dashed lines in the figure, and the arrow indicates the antenna pointing direction. Sector A is thus the area seen between the dashed lines to the west of site Kårhuset. Sector B and sector C are the areas southeast and northeast of site Vanadis, respectively. A more complete description of the transmitter hardware and measurement conditions can be found in [25].

---

[1] In the 2004 campaign, the phase rotations are due to drifting and unlocked local oscillators in the four mobile transmitters, while in the 2005 campaign they are due to drifting sample-rates in the D/A and A/D converters.
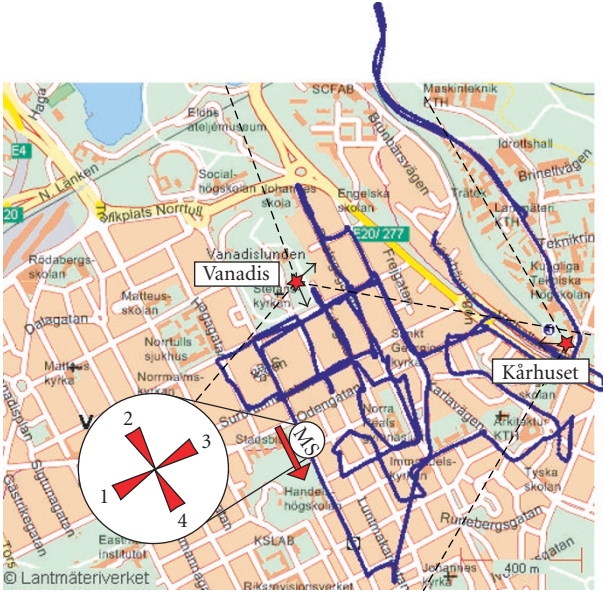
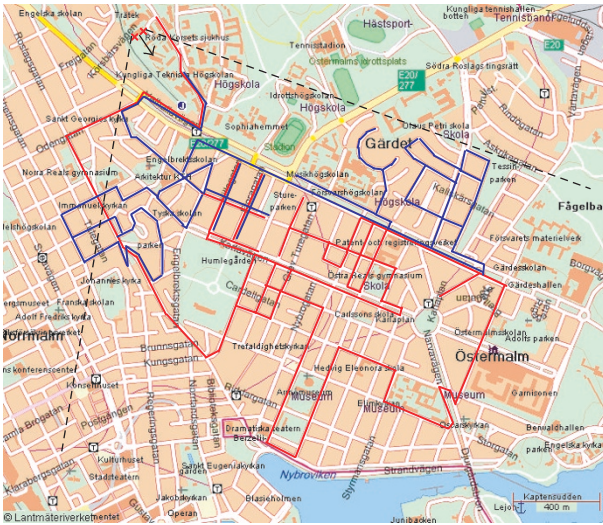FIGURE 3: Measurement geography and travelled route for 2004 campaign.

FIGURE 4: Measurement map and travelled route for the 2005 campaign.

4.4. 2005 campaign

In contrast to the previous campaign, the 2005 campaign collected data in the downlink. Two BSs with two antennas each were employed (the same type of antenna elements as in the 2004 campaign was used), each transmitting, simultaneously, one continuous tone separated 1 kHz in the 1800 MHz band. The two base stations were located on the same roof separated 50 meters, with identical boresight and therefore covering almost the same sector. The characteristics of the environment in the measured area are the same as 2004. The routes were different but with some small overlap. The MS was equipped with the 4-element box antenna as was used

in 2004, see Figure 2, to get a closer comparison between the two campaigns. In Figure 4, we see the location of the two BSs (in the upper left corner) and the measured trajectory which covered a distance of about 10 km. The arrow in the figure indicates the pointing direction of the base station antennas. The campaign measurements were conducted during two days, and the difference in color of the MS routes depicts which area was measured which day. The setups were identical on these two days.

5. PRELIMINARIES

Assume we have a system with M Tx antennas at the base station and K Rx antennas at the mobile station. Let $h_{k,m}(t)$ denote the narrow-band MIMO channel between the kth receiver antenna and the mth transmitter antenna. The narrow-band MIMO channel matrix is then defined as

$$\mathbf{H}(t) = \begin{pmatrix} h_{1,1}(t) & h_{1,2}(t) & \dots & h_{1,M}(t) \\ h_{2,1}(t) & \ddots & & \vdots \\ \vdots & & \ddots & \vdots \\ h_{K,1}(t) & \dots & \dots & h_{K,M}(t) \end{pmatrix}. \tag{3}$$

The channel is assumed to be composed of N propagation rays. The nth ray has angle of departure θ_k, angle of arrival α_k, gain g_k, and Doppler frequency f_k. The steering vector[2] of the transmitter given by $\mathbf{a}^{\text{Tx}}(\theta_k)$ and that of the receiver is $\mathbf{a}^{\text{Rx}}(\alpha_k)$. Thus, the channel is given by

$$\mathbf{H} = \sum_{k=1}^{N} g_k e^{j2\pi f_k t} \mathbf{a}^{\text{Rx}}(\alpha_k) (\mathbf{a}^{\text{Tx}}(\theta_k))^H. \tag{4}$$

The ray parameters (θ_k, α_k, g_k, and f_k) are assumed to be slowly varying and approximately constant for a distance of 30λ. Below, we define the shadow fading and the base station and the mobile station angle spread.

5.1. Shadow fading

The measured channel matrices are normalized so that they are independent of the transmitted power. The received power, P_{Rx}, at the MS is defined as

$$P_{\text{Rx}} = E|\mathbf{H}|^2 P_{\text{Tx}} = \sum_{k=1}^{N} |g_k|^2 |\mathbf{a}^{\text{BS}}(\theta_k)|^2 |\mathbf{a}^{\text{MS}}, (\alpha_k)|^2 P_{\text{Tx}}, \tag{5}$$

where P_{Tx} is the transmit power. The ratio of the received and the transmitted powers is commonly assumed to be related as [26]

$$\frac{P_{\text{Rx}}}{P_{\text{Tx}}} = \frac{K}{R^n} S_{\text{SF}}, \tag{6}$$

---

[2] The steering vector $\mathbf{a}(\theta)$ can be seen a complex-valued vector of length equal to the number of antenna elements in the array. The absolute value of the kth element is the square root of the antenna gain of that element and the phase shift of the element relative to some common reference point. That is $a_k(\theta) = \sqrt{\tilde{a}_k(\theta)} e^{j\phi_k}$.

where K is a constant, proportional to the squared norms of the steering vectors that depend on the gain at the receiver and transmitter antennas as well as the carrier frequency, base station height, and so on. The distance separating the transmitter and receiver is denoted by R. The variable S_{SF} describes the slow variation in power, usually termed shadow fading, and is due to obstacles and obstruction in the propagation path. Expressing (6) in decibels (dB) and rearranging the terms in the path loss, which describe the difference between transmitted and received powers, we have

$$
\begin{aligned}
L &= 10\log_{10}(P_{Tx}) - 10\log_{10}(P_{Rx}) \\
&= n10\log_{10}(R) - 10\log_{10}(K) - 10\log_{10}(S_{SF}),
\end{aligned}
\tag{7}
$$

where the logarithm is taken with base ten. Thus, the path loss is assumed to be linearly decreasing with log-distance separating the transmitter and receiver when measured in dB.

5.2. Base station power-weighted angle spread

The power-weighted angle spread at the base station, $\sigma_{AS,BS}^2$, is defined as

$$
\sigma_{AS,BS}^2 = \sum_{k=1}^{N} p_k (\theta_k - \overline{\theta})^2,
\tag{8}
$$

where $p_k = |g_k|^2$ is the power of the kth ray and the mean angle $\overline{\theta}$ is given by

$$
\overline{\theta} = \sum_{k=1}^{N} p_k \overline{\theta}_k.
\tag{9}
$$

5.3. Mobile station power-weighted angle spread

The power-weighted angle spread at the mobile station, $\sigma_{AS,MS}^2$, is defined as

$$
\sigma_{AS,MS}^2 = \min_{\overline{\alpha}} \left\{ \frac{1}{\sum_{k=1}^{N} p_k} \sum_{k=1}^{N} p_k (\widetilde{\mathrm{mod}}(\alpha_k - \overline{\alpha}))^2 \right\},
\tag{10}
$$

where $\widetilde{\mathrm{mod}}$ is short for modulo and defined as

$$
\widetilde{\mathrm{mod}}(\alpha) = \begin{cases} \alpha + 180, & \text{when } \alpha < -180, \\ \alpha, & \text{when } |\alpha| < 180, \\ \alpha - 180, & \text{when } \alpha > 180. \end{cases}
\tag{11}
$$

The definition of the MS angle spread is equivalent to the circular spread definition in [10, Annex A]. In the following, the power-weighted angle spread will be refereed to as the angle spread.

6. PARAMETER ESTIMATION PROCEDURES

In the measurement equipment, the receiver samples the channel on all Rx antennas simultaneously at a rate which provides approximately 35 channel realizations per wavelength. The first step of estimating the LS parameters is

TABLE 1: Number of measured 30λ segments from each measurement campaign, and number of segments in each **BS** sector.

All data 2004	S_A	S_B	S_C	All data 2005
2089	1742	1636	453	1637

to segment the data into blocks of length 30λ. This corresponds to approximately a $5m$ trajectory, during which the ray-parameters are assumed to be constant, [12], and therefore the LS parameters are assumed to be constant as well. Then smaller data sets for each BS are constructed such that they only contain samples within the given BS's sector and blocks outside the BS's sector of coverage are discarded; see definition in Section 4.3. Table 1 shows the total number of measured 30λ segments from the campaigns as well as the number of segments within each BS sector.

6.1. Estimation of shadow fading

The fast fading due to multipath scattering varies with a distance on the order of a wavelength [26]. Thus, the first step to estimate the shadow fading is to remove the fast fading component. This is done by averaging the received power over the entire $30\,\lambda$-segment and over all Tx and Rx antennas. The path loss component is estimated by calculating the least squares fit to the average received powers from all $30\,\lambda$-segments against log-distance. The shadow fading, which is the variation around a local mean, is then estimated by subtracting the distant dependent path loss component from the average received power for each local area. This estimation method for the shadow fading is the same as in, for example, [12].

6.2. Estimation of the base station power-weighted angle spread

Although advanced techniques have been developed for estimating the power-weighted angle spread, [27–29], a simple estimation procedure will be used here. Previously reported estimation procedures use information from several antenna elements where both amplitude and phase information is available. In [25], the angle spread for the 2004 data set is estimated using a precalculated look-up table generated using the gain from a beam steered towards the angle of arrival. However, as explained in Section 4.4, the BSs used in 2005 were only equipped with two antenna elements with unknown frequency offsets, and thus a beam-forming approach, or more complex estimation methods, are not applicable. Therefore, we have devised another method to obtain reasonable estimates of the angle spread applicable to both our measurement campaigns. We cannot measure the angle of departure distribution itself, thus we will only consider its second-order moment, that is, the angle of departure spread. This method is similar to the previous one [25] in that a look-up table is used for determining the angle spreads. However here the cross-correlation between the signal envelopes is used instead of the beam-forming gain.

The look-up table, which contains the correlation coefficient as a function of the angle spread and the angle of departure, has been precalculated by generating data from a model with a Laplacian (power-weighted) AoD distribution, since this distribution has been found to have a very good fit to measurement data; see, for example, [30]. The details of the look-up table generation is described in Appendix A. Note that our method is similar to the method used in [31], where the correlation coefficient is studied as a function of the angle of arrival and the antenna separation. To estimate the angle spread with this approach, only the correlation coefficient between the envelopes of the received signals at the BS and the angle to the MS is calculated, where the latter is derived using the GPS information supplied by the measurements.

For the 2005 measurements, which were conducted with two antenna elements at the BS and four antennas at the MS, the cross-correlation between the signal envelopes at the BS is averaged over all four mobile antennas as

$$c_{1,2} = \sum_{k=1}^{4} \frac{\mathrm{E}\{(|H_{k,1}| - m_{k,1})(|H_{k,2}| - m_{k,2})\}}{\sigma_{k,1}\sigma_{k,2}}, \quad (12)$$

where

$$\begin{aligned} m_{k,1} &= \mathrm{E}\{|H_{k,1}|\}, \\ m_{k,2} &= \mathrm{E}\{|H_{k,2}|\}, \\ \sigma_{k,1}^2 &= \mathrm{E}\{(|H_{k,1}| - m_{k,1})^2\}, \\ \sigma_{k,2}^2 &= \mathrm{E}\{(|H_{k,2}| - m_{k,2})^2\}. \end{aligned} \quad (13)$$

For the 2004 measurements, where also the BS had 4 antennas, the average correlation coefficient over the three antenna pairs is used.

The performance of the estimation method presented above has been assessed by generating data from the SCM model, [10], then calculating the true angle spread (which is possible on the simulated data since all rays are known) and the estimated angle spread using the method described above. The results of this comparison are shown in Figure 5. From the estimates in the figure, it is readily seen that the angle spread estimate is reasonably unbiased, with a standard deviation of 0.1 log-degrees.

6.3. Estimation of the mobile station power-weighted angle spread

At the mobile station, an estimate of the power-weighted angle spread is extracted from the power levels of the four MS antennas. Accurate estimate cannot be expected, however, the MS angle spread is usually very large due to rich scattering at ground level in this environment and reasonable estimates can still be obtained as will be seen.

A first attempt is to use a four-ray model where the AoAs of the four rays are identical to the boresights of the four MS antennas, that is, $\alpha_n = 90°(n - 2.5)$. The powers of the four rays $p_1,\ldots,p_4$ are obtained from the powers of the four antennas, that is, the Euclidean norm of the rows of the channel matrices $\mathbf{H}$. These estimates are obtained by averaging the fast fading over the 30λ segments. From the powers the angle
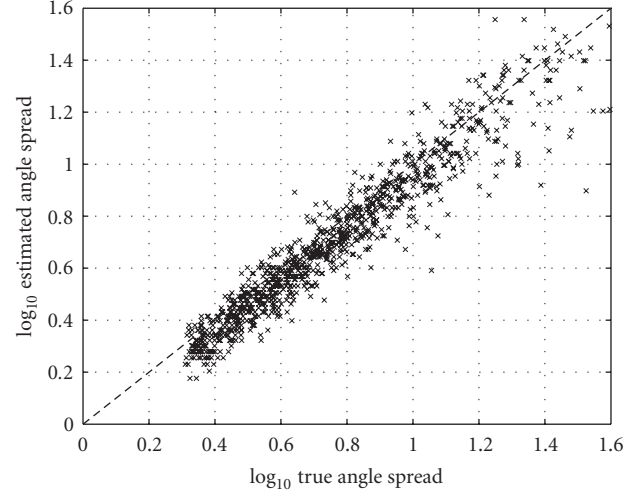

FIGURE 5: Performance of the angle spread estimator on SCM generated data.

spread is calculated using the circular model defined in (11) resulting in

$$\hat{\sigma}_{\mathrm{AS,MS\text{-}fe}}^2 = \min_{\bar{\alpha}}\left\{\frac{1}{\sum_{n=1}^4 p_n}\sum_{n=1}^4 p_n(\widetilde{\mathrm{mod}}(90(n-2.5)-\bar{\alpha}))^2\right\}, \quad (14)$$

where $(\cdot)_{\mathrm{fe}}$ is short for first-estimate. As explained in [10, Annex A], the angle spread should be invariant to the orientation of the antenna, hence, knowledge of the moving direction of the MS is not required. The performance of the estimate is first evaluated by simulating a large number of widely different cases, using the SCM model, and estimating the spread based on four directional antennas as proposed here. The result is shown in Figure 6. The details of the simulation are described in Appendix B.

The results show that the angle spread is often overestimated using the proposed method. However, as indicated by Figure 6, a better second estimate $(\cdot)_{\mathrm{se}}$ is obtained by the following compensation:

$$\hat{\sigma}_{\mathrm{AS,MS\text{-}se}}^2 = \frac{(\hat{\sigma}_{\mathrm{AS,MS\text{-}fe}}^2 - 30)100}{70}. \quad (15)$$

The performance of this updated estimator is shown in Figure 7. The second estimate is reasonable when $\hat{\sigma}_{\mathrm{AS,MS\text{-}se}}^2 > 33$. When $\hat{\sigma}_{\mathrm{AS,MS\text{-}se}}^2 < 33$, the true angle spread may be anywhere from zero and $\hat{\sigma}_{\mathrm{AS,MS\text{-}se}}^2$. For small angle spreads, problems occur since all rays may fall within the bandwidth of a single-antenna. The estimated angle spread from our measurements at the MS is usually larger than 33°, thus this drawback in the estimation method has little impact on the final result. From the estimates in Figure 7, it is readily seen that the angle spread estimate is unbiased, with a standard deviation of 6 degrees.
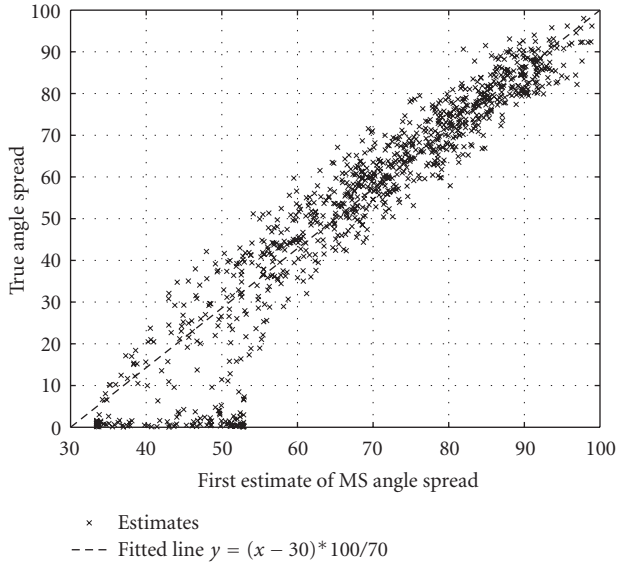
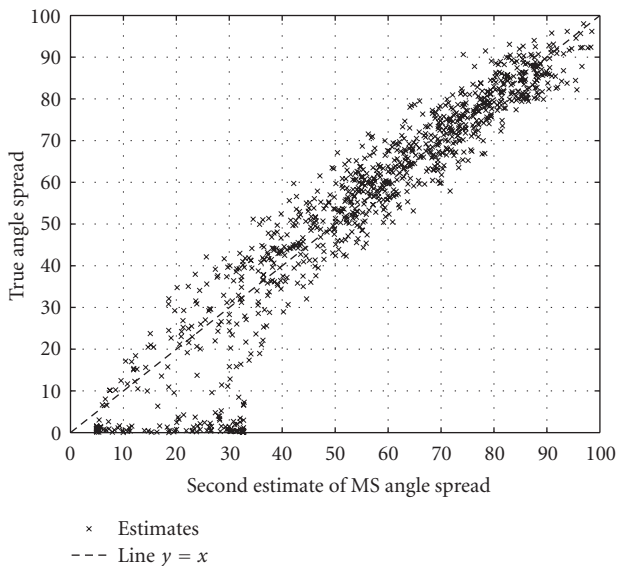FIGURE 6: Performance of the first mobile station angle spread estimate.

FIGURE 7: Performance of the second mobile station angle spread estimate.

7. RESULTS

In this section, the results of the analysis are presented in three parts. First the statistical information of the parameters is shown followed by their autocorrelation and cross-correlation properties.

7.1. Statistical properties

The first- and the second-order statistics of the LS parameters are estimated and shown in Table 3. The standard deviation of the shadow fading is given in dB while the angle spread at the BS is given in logarithmic degrees. Further, the MS an-

TABLE 2: Parmeters α and β for the beta best fit distribution to the angle spread at the mobile.

	2004:A	2004:B	2004:C	2005:1	2005:2
α	8.69	5.74	4.22	6.85	7.07
β	2.85	2.36	2.44	2.72	2.77

gle spread is given in degrees. The mean value of the shadow fading component is not tabulated since it is zero by definition. As seen from the histograms in Figure 8, which shows the statistics of the LS parameters for site 2004:B, the shadow fading and log-angle spread can be well modeled with a normal distribution. This agrees with observations reported in [12, 26]. The angle spread at the mobile on the other hand is better modeled by a scaled beta distribution, defined as

$$f(x, \alpha, \beta) = \frac{1}{B(\alpha, \beta)} \left(\frac{x}{\eta} \right)^{\alpha-1} \left(1 - \frac{x}{\eta} \right)^{\beta-1}, \qquad (16)$$

where $\eta = 360/\sqrt{12}$ is a normalization constant, equal to the maximum possible angle spread. The best fit shape parameters α and β for each of the measurement sets are tabulated in Table 2. The parameter $B(\alpha, \beta)$ is a constant which depends on α and β such that $\int_0^\eta f(x, \alpha, \beta)dx = 1$. The distributions of the parameters from all the other measured sites are similar, with statistics given in Table 3. From the table it is seen that the angle spread clearly depends on the height of the BS. The highest elevated BS, 2004:B, has the lowest angle spread and correspondingly, the BS at rooftop level, 2004:A, has the largest angle spread. The mean angle spreads at the base station are quite similar to the typical urban sites in [12] (0.74–0.95) and to those of the SCM urban macromodel (0.81–1.18) [10]. Furthermore, the standard deviations of the angle spread and the shadow fading found here, see Table 3, are somewhat smaller than those of [12]. One explanation for this could be that the measured propagation environments in 2004 and 2005 are more uniform than those measured in [12].

7.2. LS autocorrelation

The rate of change of the LS parameters is investigated by estimating the autocorrelation as a function of distance travelled by the MS. The autocorrelation functions for the large-scale parameters are shown in Figures 9 and 10, where the correlation coefficient between two variables is calculated as explained in Appendix C. Note that the autocorrelation functions can be well approximated by an exponential function with decorrelation distances as seen in Table 4. The decorrelation distance is defined as the distance for which the correlation has decreased to e^{-1}. Furthermore, it can be noted that these distances are very similar for the 2004 and the 2005 measurements, which is reasonable since the environments are similar. The exponential model has been proposed before, see [12], for the shadow fading and angle spread at the BS. The results shown herein indicate that this is a good model for the angle spread at the MS as well.

TABLE 3: Inter-BS correlation for measurement campaign 2004 site A.

	2004:A	2004:B	2004:C	2005:1	2005:2
std[SF]	5.6 dB	5.2 dB	5.4 dB	4.9 dB	4.9 dB
$E[\hat{\sigma}_{AS,BS}]$	1.2 ld	0.91 ld	0.85 ld	0.96 ld	0.87 ld
std$[\hat{\sigma}_{AS,BS}]$	0.25 ld	0.2 ld	0.23 ld	0.19 ld	0.17 ld
$E[\hat{\sigma}_{AS,MS}]$	75.1 deg	70.6 deg	65.9 deg	71.6 deg	72.2 deg
std$[\hat{\sigma}_{AS,MS}]$	15.7 deg	18.7 deg	19.2 deg	16.1 deg	16.9 deg

TABLE 4: Average decorrelation distane in maters for the estimated large-scale parameters.

	SF	$\hat{\sigma}_{AS,BS}$	$\hat{\sigma}_{AS,MS}$
$d_{decorr}(m)$	113	88	32

TABLE 5: Intra-BS correlation of LS parameters for measurement campaign 2004 site A.

	2004:A		
	SF	$\hat{\sigma}_{AS,MS}$	$\hat{\sigma}_{AS,BS}$
SF	1.00	−0.37	−0.46
$\hat{\sigma}_{AS,MS}$	−0.37	1.00	0.10
$\hat{\sigma}_{AS,BS}$	−0.46	0.10	1.00

7.3. Intrasite correlation

The intrasite correlation coefficients between different large-scale parameters at the same site are calculated for the two separate measurement campaigns. In Tables 5 and 6, the correlation coefficients for the two base stations, sectors A and B, from 2004 are shown, respectively. The last sector (C) is not shown since it is very similar to B and these parameters are based on a much smaller set of data, see Table 1. In Table 7, the same results are shown for the 2005 measurements. Since sites (2005:1 and 2005:2) show similar results and are from similar environments, the average correlation of the two is shown. It follows from mathematics that these tables are symmetrical, and in fact they only contain three significant values. The reason for showing nine values, instead of three, is to ease comparison with the intersite correlation coefficients shown in Tables 8–10. As seen from the tables, the angle spread is negatively correlated with shadow fading as was earlier found in for example [3, 12]. The cross-correlation coefficient between the shadow fading and base station angle spread is quite close to that of [12], that is −0.5 to −0.7. For the two cases where the BS is at rooftop level, Kårhuset, 2004:A, and the 2005 sites, there is no correlation between the angle spreads at the MS and the BS. However, for Vanadis, 2004:B, there is a positive correlation of 0.44. A possible explanation is that the BS is elevated some 10 meters over average rooftop height. Thus, no nearby scatterers exist and the objects that influence the angle spread at the BS are the same as the objects that influence the angle spread at the MS. A BS at rooftop on the other hand may have some nearby scatterers that will affect the angle of arrival and spread. In Figure 11, this is explained graphically. The stars are some of
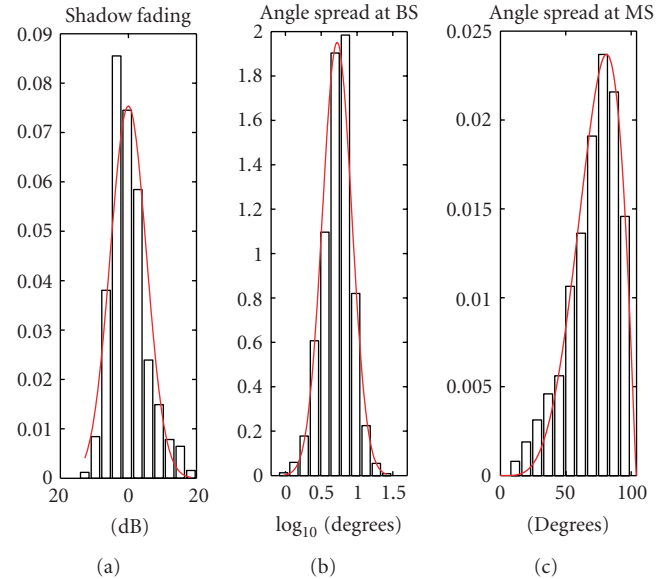

FIGURE 8: Histograms of the estimated large-scale parameters for site 2004:B.

the scatterers and the dark section of the circles depicts the area from which the main part of the signal power comes, that is the angle spread. In the left half of the picture, we see an elevated BS, without close scatterers, and therefore a large MS angle spread results in a large BS spread. In the right half of Figure 11, a BS at rooftop is depicted, with nearby scatterers, and we see how a small angle spread at the MS can result in a large BS angle spread (or the other way around).

7.4. Inter-BS correlation

The correlation coefficients between large-scale parameters at two separate sites are calculated for the data collected from both measurement campaigns. Only the data points which are common to both base station sectors, $S_i \cap S_j$, are used for this evaluation, that is, points that are within the ±60° beamwidth of both sites. As seen in section 4, describing the measurement campaigns, there is no overlap between site 2004:B and 2004:C if one considers ±60° sectors. For this specific case, the sector is defined as the area within ±70° of the BS's boresight, thus resulting in a 20° sector overlap. The results of this analysis are displayed in Tables 8, 9, and 10 for 2004:A-B, B-C, and 2005:1-2, respectively. As earlier shown in [20], the average correlation between the two sites 2004:A
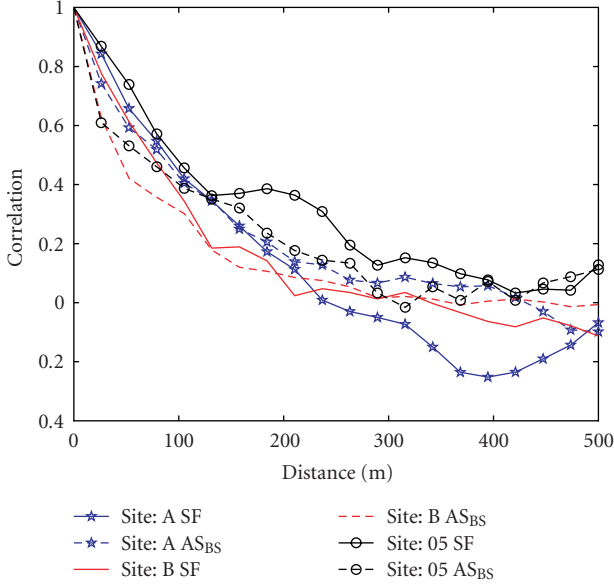
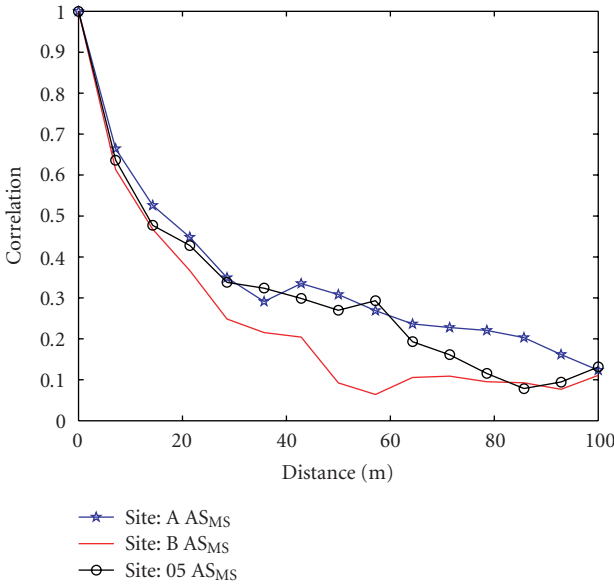Figure 9: Autocorrelation of the shadow fading and the angle spread at the base station for both measurements.

Figure 10: Autocorrelation of the angle spread at the mobile station for both measurements.
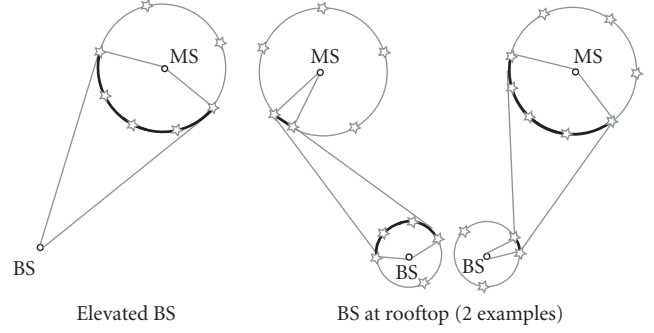

Figure 11: Model of correlation between angle spread at base station and mobile station.

Table 6: Intra-BS correlation of LS parameters for measurement campaign 2004 site B.

| | 2004:B | | |
	SF	$\hat{\sigma}_{AS,MS}$	$\hat{\sigma}_{AS,BS}$
SF	1.00	−0.54	−0.69
$\hat{\sigma}_{AS,MS}$	−0.54	1.00	0.44
$\hat{\sigma}_{AS,BS}$	−0.69	0.44	1.00

Table 7: Intra-BS correlation of LS parameters for measurement campaign 2005.

| | 2005 | | |
	SF	$\hat{\sigma}_{AS,MS}$	$\hat{\sigma}_{AS,BS}$
SF	1.00	−0.25	−0.59
$\hat{\sigma}_{AS,MS}$	−0.25	1.00	0.11
$\hat{\sigma}_{AS,BS}$	−0.59	0.11	1.00

Table 8: Inter-BS correlation of all studied LS parameters between site A and site B from 2004 measurements.

| | | 2004:A | | |
		SF	$\hat{\sigma}_{AS,MS}$	$\hat{\sigma}_{AS,BS}$
	SF	−0.14	0.08	−0.06
2004:B	$\hat{\sigma}_{AS,MS}$	−0.07	−0.05	0.03
	$\hat{\sigma}_{AS,BS}$	−0.04	−0.09	0.07

Table 9: Inter-BS correlation of all studied LS parameters between site B and site C from 2004 measurements.

| | | 2004:B | | |
		SF	$\hat{\sigma}_{AS,MS}$	$\hat{\sigma}_{AS,BS}$
	SF	0.83	−0.23	−0.52
2004:C	$\hat{\sigma}_{AS,MS}$	−0.19	0.53	0.18
	$\hat{\sigma}_{AS,BS}$	−0.54	0.22	0.31

and 2004:B is close to zero. This is not surprising since the angular separation is quite large and the environments at the two separate sites are different. The correlations between sectors B and C of 2004 are similar as between sectors 1 and 2 of 2005. In both cases, the two BSs are on the same roof, and separated 20 and 50 meters for 2004 and 2005, respectively. As can be seen, these tables (Tables 8–10) are not symmetric. Thus the correlation of, for example, the shadow fading at BS 2005:1 and the angle spread at BS 2005:2 is not the same as the correlation of the shadow fading of BS 2005:2 and the an-

gle spread of BS 2005:1 ($\langle SF^{2005:1}, \hat{\sigma}_{AS,BS}^{2005:2} \rangle \neq \langle SF^{2005:2}, \hat{\sigma}_{AS,BS}^{2005:1} \rangle$), and so on. This is not surprising.

In Figure 12, the correlation coefficient is plotted against the angle separating the two base stations with the mobile in the vertex. The large variation of the curve is due to a lack of data. This may be surprising in the light of the quite

TABLE 10: Inter-BS correlation of all studied LS parameters between site B1 and B2 from 2005 measurements.

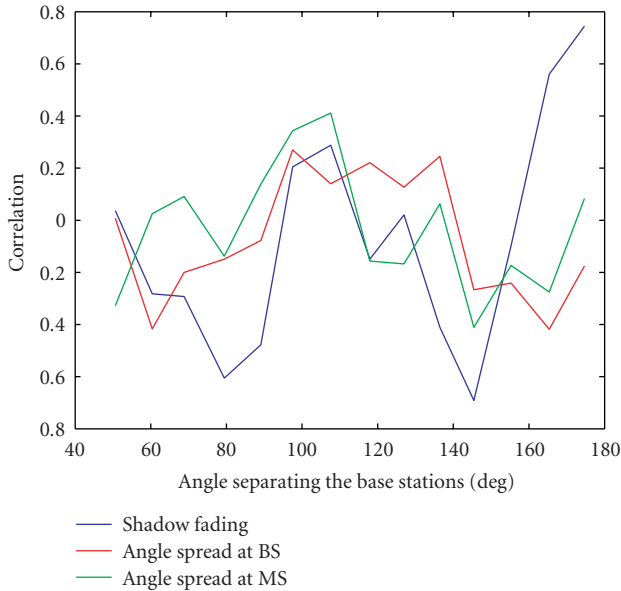|		2005:1		
		SF	$\hat{\sigma}_{AS,MS}$	$\hat{\sigma}_{AS,BS}$
	SF	0.85	−0.06	−0.45
2005:2	$\hat{\sigma}_{AS,MS}$	−0.05	0.46	0.04
	$\hat{\sigma}_{AS,BS}$	−0.27	0.18	0.33

FIGURE 12: Intersite correlation of the large-scale parameters as a function of the angle separating the base stations for the 2004 measurements.

long measurement routes. However, due to the long decorrelation distances of the LS parameters ($\sim$100 m), the number of independent observations is small. The high correlation for large angles of about 180° is mainly due to a very small data set available for this separation. Furthermore, this area of measurements is open with a few large buildings in the vicinity and thus the received power to both BSs is high.

If, on the other hand, the cross-correlation of the large-scale parameters between the two base stations from the 2005 measurements is studied, it is found that the correlation is substantial, see Table 10. Also, note that the correlation in angle spread is much smaller than the shadow fading. If the correlation is plotted as a function of the angle, separating the BSs as in Figure 13, a slight tendency of a more rapid drop in the correlation of angle spread than that of the shadow fading for increasing angles is seen. The intersite correlation results shown in Figures 12 and 13 are calculated disregarding the relative distance, see Figure 1. However, for the 2005 campaign this distance $d \approx 0$ is due to the location of the base stations.

The intersite correlation of the angle spread was calculated in the same way as the shadow fading. Only the measurement locations common to two sectors were used for these measurements. The angle spread is shown to have
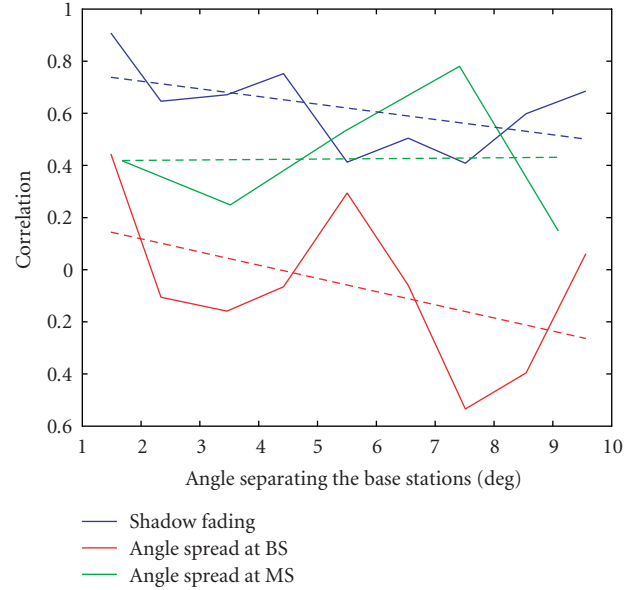

FIGURE 13: Intersite correlation of the large-scale parameters as a function of the angle separating the base stations for the 2005 measurements.

smaller correlation than the shadow fading even for small angular separations. This indicates that it may be less important to include this correlation in future wireless channel models. It should be highlighted that the correlations shown in Table 10 are for angles $\alpha < 10°$ and a relative distance $|d = \log(d_1/d_2)| \approx 0$.

8. CONCLUSION

We studied the correlation properties of the three large-scale parameters shadow fading, base station power-weighted angle spread, and mobile station power-weighted angle spread. Two limiting cases were considered, namely when the base stations are widely separated, $\sim$900 m, and when they are closely positioned, some 20–50 meters apart.

The results in [12] on the distribution and autocorrelation of shadow fading and base station angle spread were confirmed although the standard deviations of the angular spread and shadow fading were slightly smaller in our measurements. The high interbase station shadow fading correlation, when base stations are close, as observed in [13], was also confirmed in this analysis. Our results also show that angular spread correlation exists at both the base station and the mobile station if the base station separation is small. However, the correlation in angular spread is significantly smaller than the correlation of the shadow fading. Thus it is less important to model this effect. For widely separated base stations, our results show that the base station and mobile station angular spreads as well as the shadow fading are uncorrelated.

The angle spread at the mobile was analyzed and a scaled beta distribution was shown to fit the measurements well. Further, we have also found that the base station and mobile station angular spreads are correlated for elevated base

stations but uncorrelated for base station just above rooftop. Correlation can be expected if the scatters are only located close to the mobile station, which is the case for macrocellular environments, as illustrated in Figure 11.

In the future, it will be of interest to assess also the region in between the two limiting cases studied herein. Note that the limiting case of distances of 20–50 meters has a practical interest. For instance, the sectors of three-sector sites are sometimes not colocated but placed on different edges of a roof. The two base stations may also belong to different operators and the properties studied here could then be important when studying adjacent carrier interference.

APPENDICES

A. GENERATION OF ANGLE SPREAD LOOK-UP TABLE

The Laplacian angle of departure distribution is given by

$$P_A(\theta) = Ce^{(-|\theta-\theta_0|)/(\sigma_{\text{AoD}})}, \tag{A.1}$$

where θ_0 is the nominal direction of the mobile and σ_{AoD} is angle-of-departure spread. The variable C is a constant such that $\int_{-\pi}^{\pi} P_A(\theta)d\theta = 1$. When generating data, the channel covariance matrix is first estimated as

$$\mathbf{R} = \int_{\theta=-180°}^{180°} P_A(\theta)\mathbf{a}(\theta)\mathbf{a}^*(\theta)d\theta, \tag{A.2}$$

where $\mathbf{a}(\theta)$ is the array steering vector which is given by

$$\mathbf{a}(\theta) = p(\theta)\big[1, \exp\big(-j2\pi d_{\text{spacing}}\sin(\theta)\big)\big]^T, \tag{A.3}$$

$p(\theta)$ is the (amplitude) antenna element diagrams of the array, and d_{spacing} is the spacing between the antenna elements given in wavelengths. In our case the element diagrams are approximated by

$$p^2(\theta) = \max(10^{1.4}\cos^2(\theta), 10^{-0.2}), \tag{A.4}$$

and the antenna element spacing is 0.56 wavelength. The procedure for calculating the look-up table is then (1) fix angle spread and nominal angle of arrival, (2) calculate the covariance matrix $\mathbf{R}$ and it is eigendecomposition, (3) generate data from the model and calculate the envelope correlation.

The choice of Laplacian (power-weighted) AoD distribution over others, such as the Gaussian one, does only affect the estimation results marginally due to the short antenna spacing distance. This is further explained in [31].

B. EVALUATION OF THE MOBILE STATION ANGLE SPREAD ESTIMATOR

To test the estimator of the (power-weighted) RMS angle spread at the mobile-station side, some propagation channels were generated. Each channel had random number of clusters which was equally distributed between 1 and 10. The AoA of each cluster is uniformly distributed between 0° and 360°. The powers of the clusters are log-normally distributed with a standard deviation of 8 dB. Each cluster is modeled

with between 1 and 100 rays (all with equal power) which are uniformly distributed within the cluster width. The cluster widths are uniformly distributed between 0 and 10 degrees. One-thousand propagation (completely independent) channels are drawn from this model. The powers of the four antennas are calculated based on the powers of the rays, their angle of arrival, and the antenna pattern. The true angle spread is first estimated as described in [10, Annex A], and then the estimation method described in Section 6.3 is applied.

C. LARGE SCALE CORRELATIONS

The correlation coefficient between two variables is defined by the normalized covariance as

$$\rho = \langle a, b \rangle = \frac{\mathrm{E}[ab] - m_a m_b}{\sqrt{\left(\mathrm{E}[a^2] - m_a^2\right)\left(\mathrm{E}[b^2] - m_b^2\right)}}. \tag{C.5}$$

At all times when calculating the cross-correlation between LS parameters, even for small subsets of data, like when analyzing the correlation as a function of angular separation between BSs, the mean values are global. Hence the values m_a and m_b are calculated using the full data set of each BSs sector, respectively. If the mean values would be estimated locally, it is equal to assuming that the parameters are locally zero mean, and this is not what we are studying. What we want to investigate is if one parameter is large (or small) given the other.

REFERENCES

[1] G. Foschini and M. J. Gans, "On limits of wireless communications in a fading environmen when using multiple antennas," *Wireless Personal Communications*, vol. 6, no. 3, pp. 311–335, 1998.

[2] I. E. Telatar, "Capacity of multi-antenna Gaussian channels," *European Transactions on Telecommunications*, vol. 10, no. 6, pp. 585–595, 1999.

[3] D. S. Baum, H. El-Sallabi, T. Jämsä, et al., "IST-WINNER D5.4, final report on link and system level channel models," http://www.ist-winner.org/, October 2005.

[4] D. Chizhik, J. Ling, P. Wolniansky, R. Valenzuela, N. Costa, and K. Huber, "Multiple-input-multiple-output measurements and modeling in manhattan," *IEEE Journal on Selected Areas in Communication*, vol. 21, no. 3, pp. 321–331, 2003.

[5] V. Eiceg, H. Sampath, and S. Catreux-Erceg, "Dual-polarization versus single-polarization MIMO channel measurement results and modeling," *IEEE Transactions on Wireless Communications*, vol. 5, no. 1, pp. 28–33, 2006.

[6] P. Kyritsi, D. C. Cox, R. A. Valenzuela, and P. W. Wolniansky, "Correlation analysis based on MIMO channel measurements in an indoor environment," *IEEE Journal on Selected Areas in Communications*, vol. 21, no. 5, pp. 713–720, 2003.

[7] M. Steinbauer, A. F. Molisch, and E. Bonek, "The double-directional radio channel," *IEEE Antennas and Propagation Magazine*, vol. 43, no. 4, pp. 51–63, 2001.

[8] R. Stridh, K. Yu, B. Ottersten, and P. Karlsson, "MIMO channel capacity and modeling issues on a measured Indoor radio channel at 5.8 GHz," *IEEE Transactions on Wireless Communications*, vol. 4, no. 3, pp. 895–903, 2005.

[9] J. Wallace and M. Jensen, "Time-varying MIMO channels: measurement, analysis, and modeling," *IEEE Transactions on Antennas and Propagation*, vol. 54, no. 11 ,part 1, pp. 3265–3273, 2006.

[10] 3GPP-SCM, "Spatial channel model for multiple input multiple output (MIMO) simulations," *TR.25.966 v.6.10*, http://www.3gpp.org/, September 2003.

[11] M. Gudmundson, "Correlation model for shadow fading in mobile radio systems," *IEEE Electronics Letters*, vol. 27, no. 23, pp. 2145–2146, 1991.

[12] A. Algans, K. I. Pedersen, and E. P. Mogensen, "Experimental analysis of the joint statistical properties of azimuth spread, delay spread, and shadow fading," *IEEE Journal on Selected Areas in Communications*, vol. 20, no. 3, pp. 523–531, 2002.

[13] V. Graziano, "Propagation correlation at 900MHz," *IEEE Transactions on Vehicular Technology*, vol. 27, no. 4, pp. 182–189, 1978.

[14] J. Weitzen and T. J. Lowe, "Measurement of angular and distance correlation properties of log-normal shadowing at 1900 MHz and its application to design of PCS systems," *IEEE Transactions on Vehicular Technology*, vol. 51, no. 2, pp. 265–273, 2002.

[15] A. Mawira, "Models for the spatial correlation functions of the (log)-normal component of the variability of VHF/UHF field strength in urban environment," in *Proceedings of the 3rd IEEE International Symposium on Personal, Indoor and Mobile Radio Communications (PIMRC '92)*, pp. 436–440, Boston, Mass, USA, October 1992.

[16] K. Zayana and B. Guisnet, "Measurements and modelisation of shadowing cross-correlationsbetween two base-stations," in *IEEE International Conference on Universal Personal Communications (ICUPC '98)*, vol. 1, pp. 101–105, Florence, Italy, October 1998.

[17] E. Perahia, D. C. Cox, and S. Ho, "Shadow fading cross correlation between basestations," in *The 53rd IEEE Vehicular Technology Conference (VTC '01)*, vol. 1, pp. 313–317, Rhodes, Greece, May 2001.

[18] H. W. Arnold, D. C. Cox, and R. R. Murray, "Macroscopic diversity performance measured in the 800-MHz portable radio communications environment," *IEEE Transactions on Antennas and Propagation*, vol. 36, no. 2, pp. 277–281, 1988.

[19] T. Klingenbrunn and P. Mogensen, "Modelling cross-correlated shadowing in network simulations," in *The 50th Vehicular Technology Conference (VTC '99)*, vol. 3, pp. 1407–1411, Amsterdam, The Netherlands, September 1999.

[20] N. Jaldén, P. Zetterberg, M. Bengtsson, and B. Ottersten, "Analysis of multi-cell MIMO measurements in an urban macrocell environment," in *General Assembly of International Union of Radio Science (URSI '05)*, New Delhi, India, October 2005.

[21] L. Garcia, N. Jaldén, B. Lindmark, P. Zetterberg, and L. D. Haro, "Measurements of MIMO capacity at 1800MHz with in- and outdoor transmitter locations," in *Proceedings of the European Conference on Antennas and Propagation (EuCAP '06)*, Nice, France, November 2006.

[22] L. Garcia, N. Jaldin, B. Lindmark, P. Zetterberg, and L. D. Haro, "Measurements of MIMO indoor channels at 1800MHz with multiple indoor and outdoor base stations," *EURASIP Journal on Wireless Communication and Networking*, vol. 2007, Article ID 28073, 10 pages, 2007.

[23] P. Zetterberg, "WIreless DEvelopment LABoratory (WIDE-LAB) equipment base," Signal Sensors and Systems (KTH), *iR-SB-IR-0316*, http://www.ee.kth.se/, August 2003.

[24] http://www.hubersuhner.com/.

[25] P. Zetterberg, N. Jaldén, K. Yu, and M. Bengtsson, "Analysis of MIMO multi-cell correlations and other propagation issues based on urban measurements," in *Proceedings of the 14th IST Mobile and Wireless Communications Summit*, Dresden, Germany, June 2005.

[26] T. Rappaport, *Wireless Communications: Principles and Practice*, Prentice-Hall, Upper Saddle River, NJ, USA, 1996.

[27] T. Trump and B. Ottersten, "Estimation of nominal direction of arrival and angular spread using an array of sensors," *Signal Processing*, vol. 50, no. 1-2, pp. 57–69, 1996.

[28] M. Bengtsson and B. Ottersten, "Low-complexity estimators for distributed sources," *IEEE Transactions on Signal Processing*, vol. 48, no. 8, pp. 2185–2194, 2000.

[29] M. Tapio, "Direction and spread estimation of spatially distributed signals via the power azimuth spectrum," in *Proceedings of IEEE International Conference on Acoustics, Speech, and Signal Processing (ICASSP '02)*, vol. 3, pp. 3005–3008, Orlando, Fla, USA, May 2002.

[30] K. I. Pedersen, P. E. Mogensen, and B. H. Fleury, "A stochastic model of the temporal and azimuthal dispersion seen at the base station in outdoor propagation environments," *IEEE Transactions on Vehicular Technology*, vol. 49, no. 2, pp. 437–447, 2000.

[31] N. Jaldén, "Analysis of radio channel measurements using multiple base stations," Licenciate Thesis, Royal Institute of Technology, Stockholm, Sweden, May 2007.